

strain of the liquid angle θ_L : While the contact angle on (stiff) glassy polymers varies with the external strain, no variation of θ_L was found for (soft) elastomers up to 100% strain.

Exact wetting conditions from variational analysis.— Here we set out to derive the complete set of equilibrium conditions for soft wetting, by minimizing the sum of elastic and capillary energies. The geometry is sketched in Fig. 1, showing the three interfaces near the contact line. The index $i = 1$ refers to the solid-vapor interface, $i = 2$ refers to the solid-liquid interface, and $i = 3$ refers to the liquid-vapor interface. From the outset we consider that the size of elastic deformation $\sim \gamma/G$ is large compared to molecular scales (G being the static shear modulus), so that a wetting ridge develops and the interfaces are sharp. The free energy per unit width reads

$$\mathcal{F} = \mathcal{F}_e + \sum_i \int_{-\infty}^{r_i} \gamma_i(\epsilon_i) ds, \quad (2)$$

where \mathcal{F}_e is the elastic energy, and s is the curvilinear coordinate along each of the interfaces. The integrals run from a position far from the contact line (“ $-\infty$ ”) to the contact line ($s = r_i$). The strain field ϵ_i is defined for the elastic interfaces ($i = 1, 2$) and is actually a function of the reference coordinate S . This coordinate refers to a material point at the interface in its undeformed state prior to the deposition of the liquid drop. The geometric connection between the deformed state and reference state (Fig. 1) reads $ds = (1 + \epsilon_i)dS$. Hence, the variation of surface energy gives $\delta[\gamma_i(\epsilon_i)ds] = \Upsilon \delta\epsilon_i(S)dS$, with Υ_i as defined in Eq. (1). The interfaces are fully specified when complementing the strain with the local angle $\theta_i(S)$, which must also be varied to obtain the equilibrium. Minimization of \mathcal{F} then implies $\delta\mathcal{F}_e/\delta\epsilon_i + \Upsilon_i = 0$ and $\delta\mathcal{F}_e/\delta\theta_i = 0$.

It is convenient to express the derivatives of the elastic energy in terms of the elastic traction $\vec{\sigma}$, defined as the elastic force per unit (deformed) area. It can be inferred from the variation of interface displacements $\delta\vec{u}$, as derived in the Supplemental Material [23]. From the kinematic connection between $\delta\epsilon$, $\delta\theta$, and $\delta\vec{u}$, one finds (omitting the indices $i = 1, 2$)

$$\vec{\sigma}(s) = \frac{\delta\mathcal{F}_e}{\delta\vec{u}(s)} = -\frac{d}{ds} \left(\frac{\delta\mathcal{F}_e}{\delta\epsilon(S)} \vec{t} + \frac{1}{1 + \epsilon} \frac{\delta\mathcal{F}_e}{\delta\theta(S)} \vec{n} \right). \quad (3)$$

Here \vec{t} and \vec{n} , respectively, are tangential and normal unit vectors along the interfaces. Combined with the mentioned conditions for $\delta\mathcal{F} = 0$, the traction (3) becomes

$$\vec{\sigma}(s) = \frac{d(\Upsilon\vec{t})}{ds} = \Upsilon \frac{d\theta}{ds} \vec{n} + \frac{d\Upsilon}{ds} \vec{t}. \quad (4)$$

The elastic traction $\vec{\sigma}$ balances the normal Laplace pressure due to curvature, as in liquid capillarity and tangential

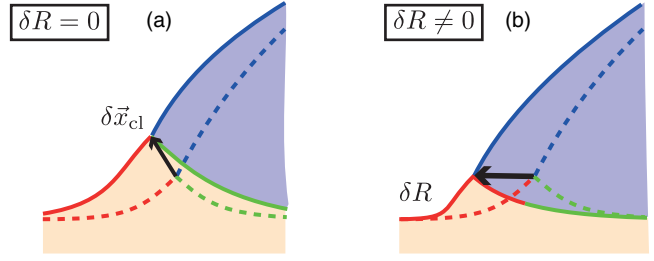


FIG. 2. Equilibrium requires that the energy is stationary with respect to any possible mode of contact line displacement, as sketched in panels (a) and (b). (a) Displacement mode at fixed material point ($\delta R = 0$), where the molecules from each phase joining at the contact line are moved together, gives rise to the Neumann condition (5). (b) Displacement mode with variable material point ($\delta R \neq 0$) gives rise to a no-pinning condition (6). Color indicates whether material points prior to displacement belonged to the wet part (green) or dry part (red) of the solid. At equilibrium, both Eqs. (5) and (6) must be satisfied.

Marangoni stress due to gradients of surface tension, originating here from inhomogeneities of $\epsilon(S)$.

The key purpose of the analysis, however, is to derive the *boundary* conditions at the contact line. For this we need to specify how the three interfaces $i = 1, 2, 3$ are connected at their respective end points at $S = R_i$. Obviously, the interfaces meet at a common position \vec{x}_{cl} (Fig. 1), which must be imposed as a constraint. The constraint does not affect Eq. (4), but is crucial for the boundary conditions that are obtained by virtual displacements of the contact line. A first mode of displacement consists of varying the contact line position $\delta\vec{x}_{cl}$ while keeping the material coordinates at the contact line fixed [$\delta R_i = 0$, see Fig. 2(a)]. This gives a boundary condition evaluated at the contact line (Supplemental Material [23]):

$$\sum \Upsilon_i \vec{t}_i = \vec{0}. \quad (5)$$

This is the Neumann law that determines θ_S , commonly used but here derived from variational principles. Importantly, Eq. (5) is obtained by a variation of the contact line position while keeping $S = R_1$ and $S = R_2$ constant; i.e., the three-phase system surrounding the contact line is displaced as a whole, without relative motion [Fig. 2(a)]. The free energy, however, should not only be minimized when the contact line is materially displaced by $\delta\vec{x}_{cl}$, but in addition when the liquid at the contact line is moved with respect to the solid. In the absence of contact line pinning (no heterogeneities of the substrate), one should therefore consider changes of the material point below the contact line. As is illustrated in Fig. 2(b), the liquid can freely move and change the solid molecules that are present at \vec{x}_{cl} . This must be accounted for by allowing the variation $\delta R_1 = -\delta R_2$, exchanging material points from the dry ($i = 1$) to the wetted interface ($i = 2$). The variation δR gives a new boundary condition at the contact line, which will be referred to as the *no-pinning* condition:

$$\Delta \left[(1 + \epsilon)^2 \gamma'(\epsilon) - \frac{\partial \mathcal{F}_e}{\partial R} \right] = 0. \quad (6)$$

Here $\Delta[\dots]$ denotes the difference between both sides of the contact line along the solid (Supplemental Material [23]). Equilibrium thus imposes two boundary conditions (5) and (6), both of which must be satisfied. Although the appearance of two conditions is logically associated with the position \vec{x}_{cl} and the material coordinate of the solid R_i , Eq. (6) had never been considered so far.

The new condition can be interpreted by analogy with the equality of “chemical potentials” at a liquid-vapor interface: while the chemical potential governs the equilibrium with respect to transport of material across such an interface, Eq. (6) ensures the equilibrium with respect to transport of elastic material (by δR_i) across the contact line. For a given combination of $\gamma_{SV}(\epsilon)$ and $\gamma_{SL}(\epsilon)$, the strain must thus adapt in order to satisfy (6). This is analogous to the adaptation of liquid and vapor densities at two-phase coexistence.

In order to compare to macroscopic experiments, we need to translate these results to regions far away from the wetting ridge (Fig. 1). To this end we first integrate Eq. (4) across the contact line, which using Eq. (5) gives

$$\Upsilon_{SL} - \Upsilon_{SV} + \gamma_{LV} \cos \theta_L = \vec{e}_x \cdot \int_{-\infty}^{\infty} \vec{\sigma} ds, \quad (7)$$

$$\gamma_{LV} \sin \theta_L = \vec{e}_y \cdot \int_{-\infty}^{\infty} \vec{\sigma} ds. \quad (8)$$

This expresses the resultant force of the three surface tensions on the volume indicated in Fig. 1, which must be balanced by the elastic stress integrated over the contact line region. Besides the normal force, we recover the appearance of a tangential stress across the contact line [3,22,24]. Recombining these equations with the no-pinning condition (6) this can be expressed as

$$\begin{aligned} & (1 + \epsilon_\infty)(\gamma_{SL} - \gamma_{SV} + \gamma_{LV} \cos \theta_L) \\ & = -\Delta[(1 + \epsilon)^2 \gamma'] + \int_{-\infty}^{\infty} \vec{\sigma} \cdot [(1 + \epsilon)\vec{t} - (1 + \epsilon_\infty)\vec{e}_x] ds. \end{aligned} \quad (9)$$

This is the generalization of Young’s law for the liquid angle θ_L far away from the contact line, also applicable when the substrate is uniaxially strained to a value ϵ_∞ .

The paradox.—So far the derivation has been fully exact and provides the thermodynamic framework for partial wetting on soft solids, valid also for large deformations. Resolving the experimental controversy regarding the Shuttleworth effect calls for a quantitative prediction, and for this reason we evaluate these exact results in the framework of linear elasticity for which $|\epsilon| \ll 1$. The elastic energy is then obtained by the surface

integral $\mathcal{F}_e = \int ds \frac{1}{2} \vec{u} \cdot \vec{\sigma}$. Hence, the boundary condition (6) then simplifies to $\Delta[\gamma'(0) - \frac{1}{2} \vec{u} \cdot \vec{\sigma}] = 0$. A stress discontinuity is not admitted in linear elasticity, as it would lead to a logarithmic singularity of slope. Hence, we deduce that the newly found no-pinning condition (6) enforces continuity of $\gamma'(0)$, so that $\gamma'_{SV} = \gamma'_{SL}$. Far from the contact line this implies that Eq. (9) reduces to the standard Young equation $\gamma_{SL} - \gamma_{SV} + \gamma_{LV} \cos \theta_L = 0$. All the above remains valid for large ϵ_∞ , as long as the perturbation induced by the deposited drop remains in the regime of linear response.

This explains why θ_L *must* remain constant on stretched soft solids [10], even when the Shuttleworth effect leads to a change of θ_S , an experimental fact that has been observed by simultaneous measurement of θ_S and θ_L in PDMS in Ref. [9]. Namely, the no-pinning condition $\gamma'_{SV} = \gamma'_{SL}$ imposes that the difference $\gamma_{SV} - \gamma_{SL}$ stays constant. Hence, as long as the drop’s distortion of the solid is within linear response, the constancy of θ_L is a direct consequence of the lack of hysteresis, and as such θ_L cannot predict the absence or presence of the Shuttleworth effect on soft elastic solids. The situation is different for glassy polymers, which are much stiffer and for which changes of θ_L have been observed when stretching the substrate [10]. In that case the associated deformations $\sim \gamma/G$ are subnanometric so that the solid remains essentially flat. In our macroscopic framework, this corresponds to the rigid limit in which the droplet does not induce any elastic deformation—hence, the strain remains everywhere fixed at the experimentally imposed value ϵ_∞ . The variation of the horizontal contact line position is then naturally connected to a variation of the material point according to $\delta x_{cl} = (1 + \epsilon_\infty)\delta R$ so that the no-pinning condition (due to δR) is the same as Young’s equation (due to δx_{cl} in the rigid limit). So indeed, for stiff polymers there is no thermodynamic reason why θ_L should remain constant when the externally imposed strain ϵ_∞ is varied experimentally.

Turning back to the case of soft reticulated polymer networks, for which γ/G is significantly larger than the molecular scale, the equality $\gamma'_{SV} = \gamma'_{SL}$ at small strain is not expected to be universally obeyed. This will depend on the relevant constitutive relations $\gamma(\epsilon)$, which is a topic that is currently beginning to be explored [25,26]. One could expect the emergence of large strain at the contact line to satisfy the no-pinning condition (6). If such an equilibrium of chemical potential is not compatible with the constitutive relations, pinning must be observed. Indeed, elastomeric surfaces can exhibit a strong contact angle hysteresis, which we suggest finds its origin in the Shuttleworth effect. For example, the Wilhelmy plate experiment of Ref. [22] for which strong hysteresis was present, exhibited $\gamma'_{SL} \neq \gamma'_{SV}$ as inferred from the tangential stress balance (7).

Contact angle selection from dynamic spreading.—We now experimentally validate this interpretation framework: linear response and absence of hysteresis necessarily imply

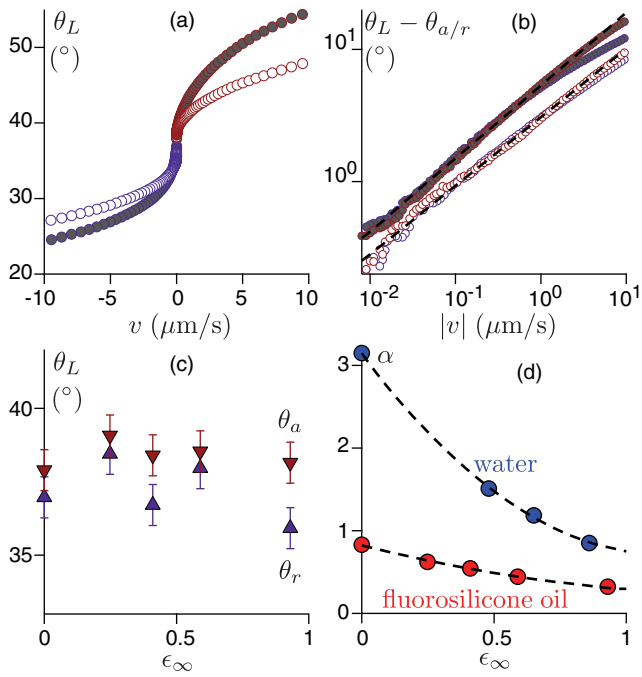


FIG. 3. Pinning and enhanced contact line mobility. (a) Liquid-vapor macroscopic contact angle θ_L with respect to the undeformed solid surface as a function of the contact line velocity v (liquid: fluorosilicone oil). Closed and open symbols: unstrained and strained ($\epsilon_\infty = 0.93$) samples respectively. (b) Contact angle rotations $\theta_L - \theta_{a/r}$ vary like v^n , with n obtained from loss modulus measurement as expected from (10) ($n = 0.55$ for $\epsilon_\infty = 0$ and $n = 0.50$ for $\epsilon_\infty = 0.93$). (c) Liquid contact angles $\theta_{a/r}$ in the limit $v \rightarrow 0^+/0^-$, as a function of the applied strain ϵ_∞ . (d) Contact line friction factor α defined by Eq. (10) as a function of strain ϵ_∞ .

the equality $\gamma'_{SV} = \gamma'_{SL}$ —and hence θ_L independent of strain. Since hysteresis plays a key role in our theory, we set out to perform a proper quantification of hysteresis. This calls for dynamic spreading experiments, where the contact angle is measured versus contact line velocity v [27]. The hysteresis is then inferred from the limit of vanishing velocity, comparing the advancing motion ($v \rightarrow 0^+$) and the receding motion ($v \rightarrow 0^-$). Here we use the same set up as in Ref. [20] to measure the macroscopic contact angle θ_L , adapted to impose a uniaxial strain ϵ_∞ to a 6 mm thick PDMS gel (Dow Corning CY52-276, prepared in 1:1 ratio) molded in a Petri dish. After curing at room temperature during 24 h, 20 mm-wide strips are cut, stretched, and clamped on a rigid plate. A liquid droplet is inflated or deflated with a syringe to impose an advancing or a receding motion, measured along the stretching direction. Milli-Q water and fluorosilicone oil (poly(3,3,3-trifluoropropylmethylsiloxane), Gelest FMS 121) were used.

The resulting liquid contact angle θ_L is shown in Fig. 3(a) as a function of the contact line velocity v , for unstrained (closed circles) and strained samples (open circles). The curves are apparently continuous at $v = 0$, pointing to a

nearly perfect absence of hysteresis. Both the advancing and receding motions exhibit a power-law dependence $\theta_L - \theta_{a/r} \sim |v|^n$ over more than two decades in velocity [Fig. 3(b)]. This allows us to determine accurately the advancing θ_a and receding θ_r angles, revealing a small ($\sim 1^\circ$) constant hysteresis [Fig. 3(c)]. Furthermore, the equilibrium liquid angle $\theta_a \simeq \theta_r$ is independent of the imposed strain ϵ_∞ , consistently with previous independent experiments [9,10]. The condition $\gamma'_{SL} = \gamma'_{SV}$, predicted by our theory in the absence of hysteresis, is therefore fulfilled in our experiment.

Another remarkable result of Fig. 3 is that the spreading velocities are strongly enhanced upon stretching the solid. Namely, comparing the data for strained (open) and unstrained (closed) samples for a given θ_L , the velocity $|v|$ is larger by a factor of 3. Hence, we observe that stretching leads to an enhanced wetting mobility. Below we demonstrate how this effect serves as a simple diagnostic for the presence of a Shuttleworth effect.

The final step is to experimentally verify our assumption of linear response and to explain the enhanced wetting mobility on a stretched gel. The gel's linear rheology under uniaxial strain turns out to only weakly depend on the imposed ϵ_∞ (Supplemental Material [23]). The loss modulus G'' depends as a power law of the angular frequency ω : $G'' \propto G(\omega\tau)^n$, where the cross-over time τ and the exponent n marginally depend on ϵ_∞ (Supplemental Material [23]). This enables us to use the dynamical theory from Ref. [20], relating θ_L to the contact line velocity v

$$\theta_L - \theta_{a/r} = \alpha \left(\frac{G|v|\tau}{\gamma_{LV} \sin \theta_L} \right)^n, \quad (10)$$

where the dimensionless friction factor α depends on the geometry of the ridge. Indeed, the exponents n measured for θ_L and in the linear rheological measurement are found to be consistent, as predicted by Eq. (10). The agreement of these exponents provides direct proof that the droplet dynamics probes the substrate within linear response, even when the prestrain ϵ_∞ is not small.

The experimentally measured friction factor α defined by Eq. (10) is reported as a function of ϵ_∞ in Fig. 3(d). The reduction of friction with strain can be attributed to the Shuttleworth effect, via a gradual increase of θ_S : A shallower wetting ridge leads to a smoother motion of material points and hence to less dissipation. This effect can be estimated from viscoelastic theory [20] (based on constant surface tensions), suggesting the scaling

$$\alpha \sim \cos^{1+n}(\theta_S/2). \quad (11)$$

Hence, the reduced friction α in our spreading experiments [Fig. 3(d)] points to a Shuttleworth-induced gradual increase of θ_S with ϵ_∞ . This is consistent with direct measurements of θ_S in Ref. [9] for a very similar PDMS

system in the static limit—for which we remind that θ_L was also found independent of strain. Obviously, an important step for future work is to achieve fully self-consistent computations of the ridge dynamics that includes the strains induced by the Shuttleworth effect. This would, e.g., lead to a fully quantitative prediction of $\alpha(\theta_S)$.

Outlook.—Our study offers a general framework that establishes the laws of wetting on deformable soft solids, and which is consistent with all experimental observations. We have shown that equilibrium, in particular the lack of hysteresis, requires the equality of Shuttleworth coefficients $\gamma'_{SL} = \gamma'_{SV}$ for both the wet and dry solid. This sheds an unexpected light on coupling of physical chemistry, encoded in $\gamma(\epsilon)$, to the mechanics of wetting, and calls for a better understanding of the molecular origin of the Shuttleworth effect in cross-linked polymer networks [25,26]. This is of prime importance for the design and rheological characterisation of extremely soft materials, for which the interfacial effects dominate over bulk elasticity. From the perspective of wetting applications, we demonstrate that the Shuttleworth effect offers a new route to control the mobility of the contact line as illustrated here by stretching-enhanced spreading velocities.

This work was financially supported by the ANR grant Smart and ERC (the European Research Council) Consolidator Grant No. 616918.

-
- [1] B. Roman and J. Bico, *J. Phys. Condens. Matter* **22**, 493101 (2010).
- [2] S. Mora, T. Phou, J.-M. Fromental, L. M. Pismen, and Y. Pomeau, *Phys. Rev. Lett.* **105**, 214301 (2010).
- [3] B. Andreotti and J. H. Snoeijer, *Europhys. Lett.* **113**, 66001 (2016).
- [4] R. W. Style, A. Jagota, C.-Y. Hui, and E. R. Dufresne, *Annu. Rev. Condens. Matter Phys.* **8**, 99 (2017).
- [5] J. Bico, É. Reyssat, and B. Roman, *Annu. Rev. Fluid Mech.* **50**, 629 (2018).
- [6] N. Naderman, C.-Y. Hui, and A. Jagota, *Proc. Natl. Acad. Sci. U.S.A.* **110**, 10541 (2013).
- [7] S. Mondal, M. Phukan, and A. Ghatak, *Proc. Natl. Acad. Sci. U.S.A.* **112**, 12563 (2015).
- [8] R. W. Style, R. Boltyanskiy, Y. Che, J. S. Wettlaufer, L. A. Wilen, and E. R. Dufresne, *Phys. Rev. Lett.* **110**, 066103 (2013).
- [9] Q. Xu, K. Jensen, R. Boltyanskiy, R. Sarfat, R. W. Style, and E. R. Dufresne, *Nat. Commun.* **8**, 555 (2017).
- [10] R. D. Schulman, M. Trejo, T. Salez, E. Raphael, and K. Dalnoki-Veress, *Nat. Commun.* **9**, 982 (2018).
- [11] R. W. Style and E. R. Dufresne, *Soft Matter* **8**, 7177 (2012).
- [12] A. Marchand, S. Das, J. H. Snoeijer, and B. Andreotti, *Phys. Rev. Lett.* **109**, 236101 (2012).
- [13] L. A. Lubbers, J. H. Weijss, L. Botto, S. Das, B. Andreotti, and J. H. Snoeijer, *J. Fluid Mech. Rapids* **747**, R1 (2014).
- [14] J. Dervaux and L. Limat, *Proc. R. Soc. A* **471**, 20140813 (2015).
- [15] Z. Cao and A. Dobrynin, *Macromolecules* **48**, 443 (2015).
- [16] A. Carré, J.-C. Gastel, and M. E. R. Shanahan, *Nature (London)* **379**, 432 (1996).
- [17] D. Long, A. Ajdari, and L. Leibler, *Langmuir* **12**, 1675 (1996).
- [18] T. Kajiyama, A. Daerr, T. Narita, L. Royon, F. Lequeux, and L. Limat, *Soft Matter* **9**, 454 (2013).
- [19] J. Dupas, E. Verneuil, M. Van Landeghem, B. Bresson, L. Forny, M. Ramaioli, F. Lequeux, and L. Talini, *Phys. Rev. Lett.* **112**, 188302 (2014).
- [20] S. Karpitschka, S. Das, M. van Gorcum, H. Perrin, B. Andreotti, and J. H. Snoeijer, *Nat. Commun.* **6**, 7891 (2015).
- [21] R. Shuttleworth, *Proc. Phys. Soc. London Sect. A* **63**, 444 (1950).
- [22] A. Marchand, S. Das, J. H. Snoeijer, and B. Andreotti, *Phys. Rev. Lett.* **108**, 094301 (2012).
- [23] See Supplemental Material at <http://link.aps.org/supplemental/10.1103/PhysRevLett.121.068003> for technical details of the variational derivations and of the experiment.
- [24] S. Das, A. Marchand, B. Andreotti, and J. H. Snoeijer, *Phys. Fluids* **23**, 072006 (2011).
- [25] H. Liang, Z. Cao, Z. Wang, and A. V. Dobrynin, *ACS Macro Lett.* **7**, 116 (2018).
- [26] Q. Xu, R. W. Style, and E. R. Dufresne, *Soft Matter* **14**, 916 (2018).
- [27] H. Perrin, R. Lhermerout, K. Davitt, E. Rolley, and B. Andreotti, *Phys. Rev. Lett.* **116**, 184502 (2016).